Advances in Geo-Energy Research

Vol. 15, No. 1, p. 55-67, 2025

Original article

Design and experimental performance evaluation of high-temperature and high-pressure test platform for deep *in-situ* fidelity coring tools

Wei Huang[1,2], Jianan Li[1,3]*, Yang Yang[3], Zhiqiang Liu[4], Delei Shang[1]

[1]*Guangdong Provincial Key Laboratory of Deep Earth Sciences and Geothermal Energy Exploitation and Utilization, College of Civil and Transportation Engineering, Shenzhen University, Shenzhen 518060, P. R. China*

[2]*School of Mechanical Engineering, Sichuan University, Chengdu 610065, P. R. China*

[3]*College of Water Resource and Hydropower, Sichuan University, Chengdu 610065, P. R. China*

[4]*Jin Shi Drill Tech Co., Ltd, Tangshan 063004, P. R. China*

Keywords:
Deep *in-situ*
fidelity coring tools
test platform
experimental study

Cited as:
Huang, W., Li, J., Yang, Y., Liu, Z., Shang, D. Design and experimental performance evaluation of high-temperature and high-pressure test platform for deep *in-situ* fidelity coring tools. Advances in Geo-Energy Research, 2025, 15(1): 55-67.
https://doi.org/10.46690/ager.2025.01.06

Abstract:
With the increasing mining depth of mineral resources, the temperature and pressure of the underground environment are also on the rise, which puts forward strict requirements for the performance of fidelity coring tools. To promote the development of such tools, a comprehensive high-temperature and high-pressure test platform for deep *in-situ* fidelity coring tools was constructed, and its working principle was described in detail. In addition, four key functional modules of the test platform were developed. On the basis of the principle of gas-liquid pressurization and the burst failure criterion of pressure vessel, a mechanical module integrating the functions of pressurization and pressure maintaining was designed. The heating and insulation module was developed by using a U-shaped high-speed heater and electromagnetic induction heating technology. The innovation utilized coil cooling technology to achieve effective cooling and pressure relief. Furthermore, the working performance of the test platform was studied experimentally. The designed test platform could run stably for more than 110 min under test conditions of high pressure and temperature of 140 MPa and 150 °C, respectively, and it could maintain a stable pressure and temperature at 200 MPa and 160 °C for more than 182 min. Under the high pressure condition of 220 MPa, the pressure remained stable within 140 min, without any fluid leakage. Therefore, the test platform designed in this study can provide experimental conditions of high pressure and high temperature for the research of fidelity coring tools, which is of great significance for the accurate evaluation and safe exploitation of deep mineral resources.

1. Introduction

As the Earth's shallow resources are gradually being exhausted, the exploitation of deeper mineral resources such as coal, oil and metal is expanding; for instance, the exploitation depth of oil has exceeded 8,800 m (Walker, 2012; Gao et al., 2022; Xie et al., 2024). With the gradual increase in mining depth, the industry faces the challenge of high temperature and high pressure, which seriously restricts the safe and efficient mining of deep resources (Gao et al., 2021; He et al., 2022; Yu et al., 2023). The acquisition of *in-situ* "fidelity cores" is an effective method to realize the effective evaluation of resource reserves and guide the safe mining of deep resources (Xie et

Yandy Scientific Press

*Corresponding author.
E-mail address: 2020323022018@stu.scu.edu.cn (W. Huang); lijn2013@163.com (J. Li); yangyang6463@126.com (Y. Yang); bblzq1980@163.com (Z. Liu); sdl18@tsinghua.org.cn (D. Shang).

Received October 18, 2024; revised November 13, 2024; accepted December 5, 2024; available online December 11, 2024.

al., 2021; Guo et al., 2023; Huang et al., 2023). However, the deep environment puts forward strict requirements for fidelity coring tools (Li et al., 2021; Wei et al., 2024; Yang et al., 2024). To promote the development of fidelity coring tools, it is urgent to design a high-temperature and high-pressure test platform for the testing of such tools.

In order to study the performance of downhole tools, scholars in relevant fields have carried out numerous experiments for the research and development of test devices (Hooker and Brigham, 1978; Kabir et al., 1996; Dou et al., 2022). According to the research needs of drilling tools, Zhang (2009) developed a downhole tool test equipment that can provide a pressure of 60 MPa and a temperature of 180 °C. The test system can heat its internal circulating fluid from room temperature to 180 °C within 4 h. Ding (2014) developed a test system that can create a test pressure of 105 MPa and a high temperature of 200 °C for the research of downhole tools. The device mainly consists of downhole simulation wellbore, heating system, wellhead sealing, and suspension system. Du and Wei (2015) designed a set of downhole tool testing device for simulating the downhole environment to verify the safety and reliability of downhole tools during operation. This device can provide a maximum test temperature of 150 °C and a maximum test pressure of 90 MPa. Zheng et al. (2017) developed a set of testing platform for downhole instruments with a working temperature of 125 °C and a working pressure of 70 MPa on the basis of constant pressure variable pump control technology to test the performance stability of measurement while drilling instruments before drilling. Liu et al. (2019) developed the DTTS-200-140 test system on the basis of the application environment of downhole tools in the Chuanyu Gas field, which can test the stability of downhole tools at a pressure of 140 MPa and a temperature of 200 °C. The test system developed by Pang et al. (2017) can provide a maximum pressure of 210 MPa, a maximum test temperature of 200 °C, and the maximum inner diameter of the test wellbore is 193.7 mm. Their device adopts the methods of liquid cylinder loading, hot air heating and independent pressure of three pressure systems, which can load the downhole tools inside the wellbore under high-temperature and high-pressure conditions and can completely simulate the whole working process of the downhole tools, ensuring that the test of the downhole tools is reliable.

Although these studies have achieved promising results, few devices exist with a maximum pressure supply capacity of 220 MPa, and even fewer test devices have been designed that provide both a pressure of 200 MPa and a temperature condition of 160 °C. Besides, even if the temperature and pressure operating conditions can be achieved, it is challenging for the testing space to meet the research requirements of deep *in-situ* fidelity coring tools. Therefore, on the basis of the testing requirements of fidelity coring tools, this paper independently developed a high-temperature and high-pressure test platform for deep *in-situ* fidelity coring tools featuring a maximum pressure supply capacity of 220 MPa, which can stably operate under the test conditions of 200 MPa and 160 °C for an extended period of time. The maximum test space inside the test platform is suitable for carrying out the testing of coring tools with a maximum diameter of 280 mm and a maximum length of 4,900 mm. Therefore, this platform can effectively promote the development of deep *in-situ* fidelity coring tools, providing technical and equipment support for the effective evaluation of deep resources reserves and the safe mining of deep resources.

Table 1. Key technical indicators of the proposed test platform.

Technical index	Parameter value
Maximum pressure	220 MPa
Coupling working index	200 MPa, 160 °C
Pressure fluctuation	$\leq \pm$ 2 MPa
Temperature fluctuation	$\leq \pm$ 3 °C

2. Structure and working principle

2.1 Technical requirements

Taking the test requirements of deep *in-situ* fidelity coring tools as a basis, the test platform should have a pressure supply capacity of up to 220 MPa, and the ability to be operated in a test environment with a pressure of 200 MPa and a temperature of 160 °C for an extended period. Meanwhile, the test space should be suitable for a fidelity coring tool with a maximum diameter of 280 mm and a maximum length of 4,900 mm. To ensure the safety of equipment and operators during the test, the designed test platform can automatically apply and maintain the target test temperature and pressure, and the test parameters can be set in stages according to the test requirements. The unloading of temperature and pressure can be completed automatically after the test. Meanwhile, the test pressure and temperature values can be recorded in real time, and the curve of pressure and temperature changes with time can be generated. The key technical indicators of the test platform are shown in Table 1.

2.2 Structure

The test platform mainly consists of a pressurization module, a heating and insulation module, a measurement and control module, a temperature and pressure unloading module, and an auxiliary device. The multiple modules work in coordination to apply and maintain the test temperature and pressure required by the fidelity coring tool, as shown in Fig. 1. The schematic diagram of the functions of each module is shown in Fig. 2. The pressurization module mainly realizes the application and maintenance of test pressure. The heating and insulation module is composed of two parts: temperature-controlled cabinet and electromagnetic induction heating system (EIHS), which work in coordination to quickly achieve the application and maintenance of test temperature. The measurement and control module collects the temperature and pressure data in the test process in real time through sensors, adjusts the test temperature and pressure according to the setting value, and displays the curve of temperature and pressure change with time in the testing process. The

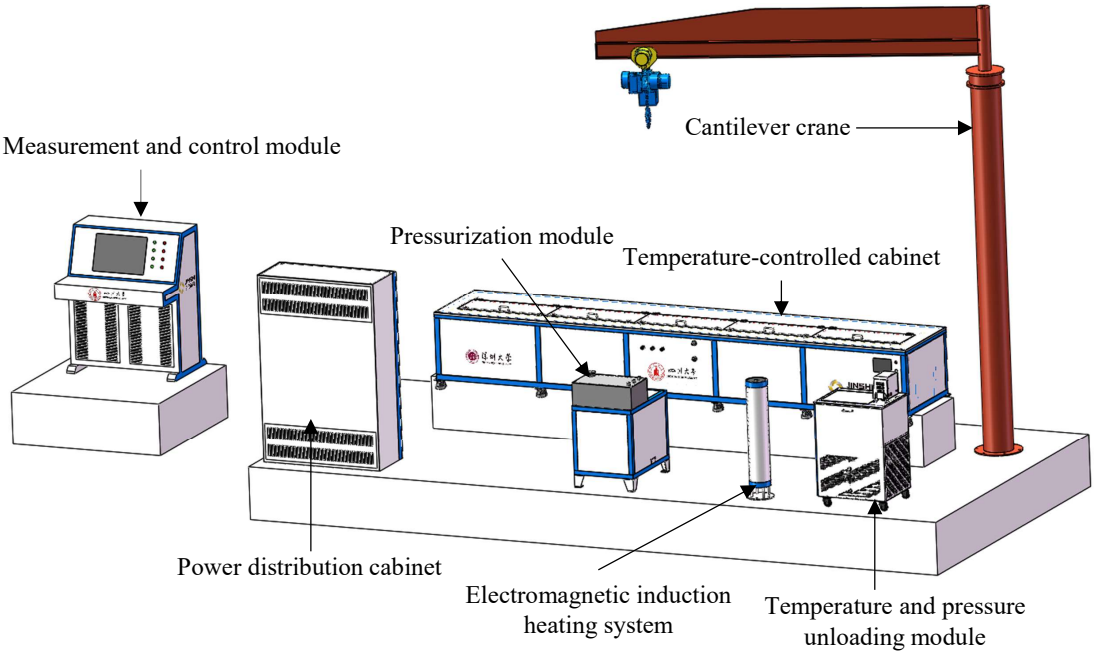

Fig. 1. Structure of the test platform.

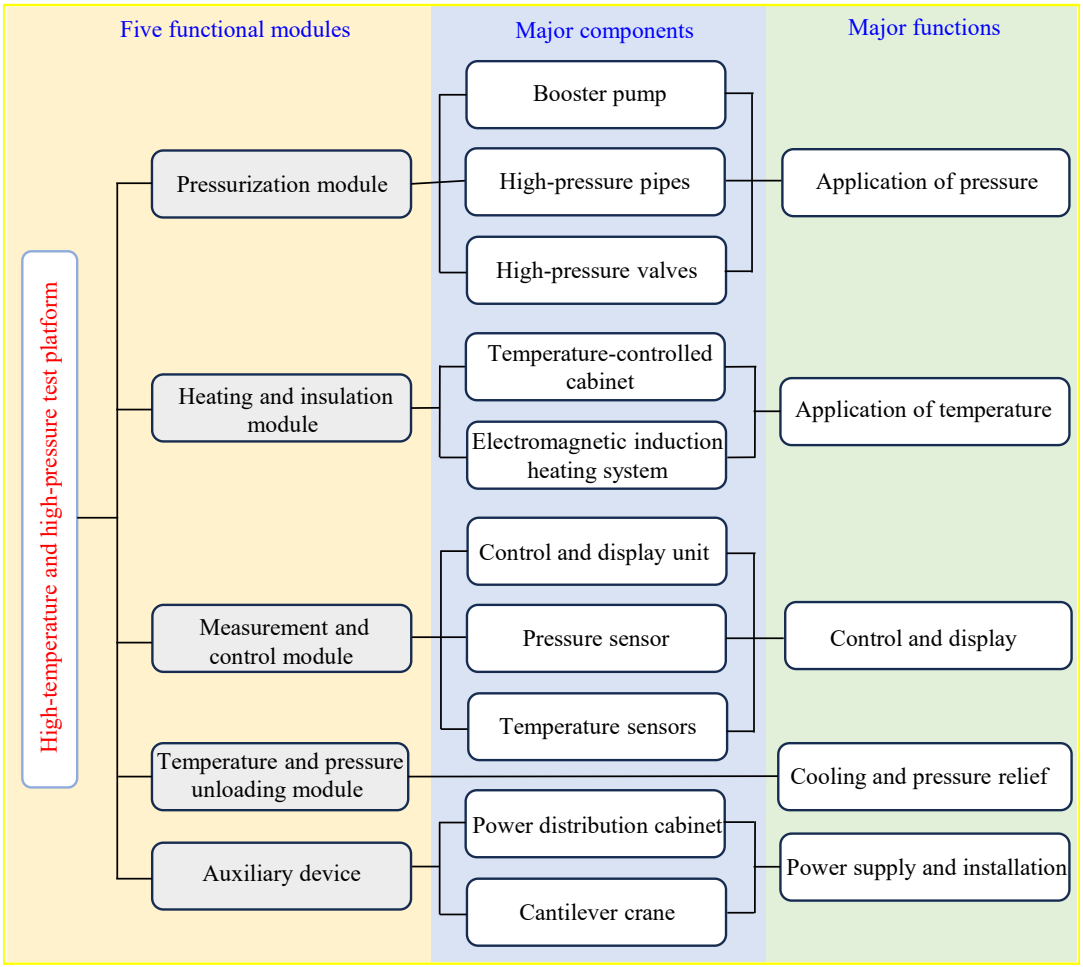

Fig. 2. Schematic diagram of the major functional modules, components and functions.

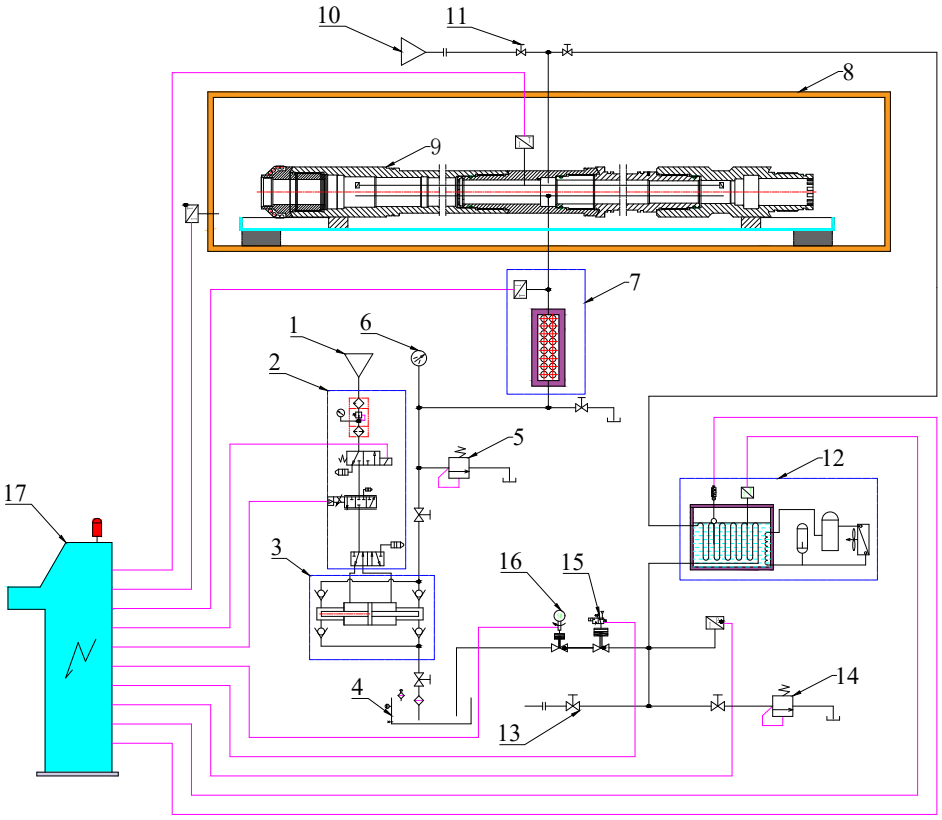

Fig. 3. Working principle diagram of the test platform. 1-Air source 1; 2-Gas valve assembly; 3-Gas-liquid booster pump; 4-Water tank; 5-Safety valve 1; 6-Pressure gauge; 7-Electromagnetic induction heating system; 8-Temperature-controlled cabinet; 9-Fidelity coring tool; 10-Air source 2; 11-Intake valve; 12-Temperature and pressure unloading module; 13-Exhaust valve; 14-Safety valve 2; 15-Pneumatic pressure relief valve; 16-Servo pressure relief valve; 17-Controlled cabinet.

temperature and pressure unloading module can safely unload the temperature and pressure after the test has been completed. The power distribution cabinet and cantilever crane are the auxiliary devices of the test platform. The power distribution cabinet is used to configure the power supply of the whole test platform. The test pieces in the studio of the temperature control box are installed by the cantilever crane.

2.3 Working principle

The working principle of the test platform is shown in Fig. 3, where the purple lines represent the control lines and the black lines represent the high-pressure pipes. The operation of the whole test system is controlled by the control and measurement module through the control lines. The pressurized gas in the air source 1 enters the gas-liquid booster pump (GLBP) through the gas valve assembly and drives the pump to extract low-pressure water from the tank and pressurize it. The pressurized water flows to the EIHS through the high pressure pipes for preliminary heating, then further flows to the test part, so that the air inside the test part is discharged through the exhaust valve. After the inside of the test part has been filled with water and the temperature is uniform, the exhaust valve is closed and the water inside the test part is heated to the target temperature by the temperature-controlled cabinet. During the heating process, the pressure of water will increase with rising temperature. If the pressure is exceeded, the safety valve 2 will automatically start to relieve pressure. Furthermore, the pump is started to increase pressure to the target value, and the heating power of the EIHS is also increased, so that the pressurized water entering the test part can be heated to the target temperature. Then, the test part to be tested is placed in the platform for an extended period to detect its stability and reliability under the set temperature and pressure values. After the test, the pneumatic pressure relief valve and servo pressure relief valve are controlled to relieve system pressure, and the high-temperature water is cooled by the temperature and pressure unloading module. Finally, the air source 2 is started and the intake valve is opened to blow the clean water inside the test part and the high pressure lines into the water tank.

3. Key functional modules

This section designed the four key functional modules of the test platform in detail, which are pressurization module, heating and insulation module, measurement and control module, and temperature and pressure unloading module.

3.1 Pressurization module

The pressurization module is composed of GLBP, high-pressure pipes, water tank, liquid indicator, high-pressure

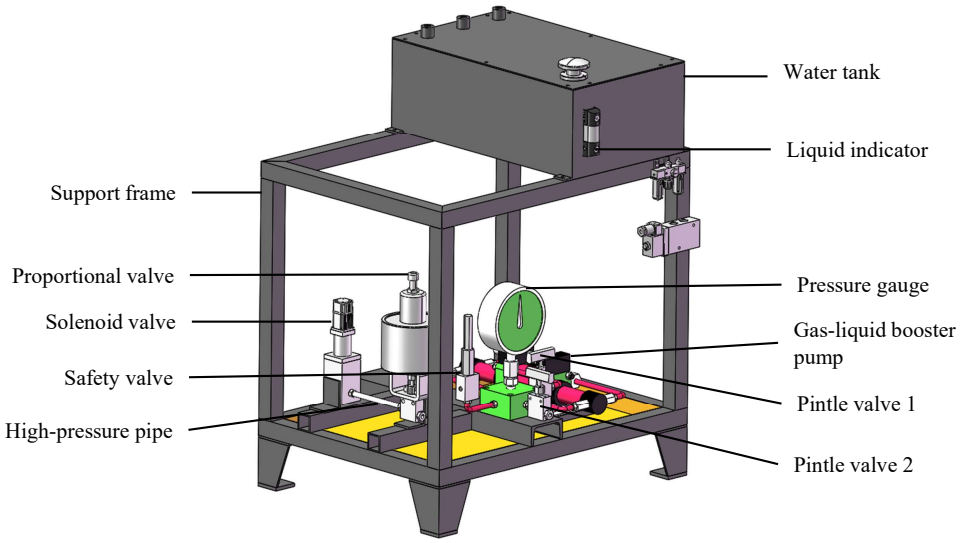

Fig. 4. Composition of the pressurization module.

valves (proportional valve, safety valve, Pintle valve, etc.), pressure gauge, and support frame, as shown in Fig. 4.

The GLBP is the core component of the pressurization module. It is a piston booster pump with compressed air as the power source, with a maximum pressure supply capacity of 220 MPa. The pump body is made of stainless steel. When the air pump is started, the spool of the booster gas control valve driven by the pressurized gas is switched reciprocally to control the piston of the GLBP to rapidly reciprocate and pump the high-pressure water. As the output pressure of the GLBP increases, the reciprocating speed of the piston gradually slows down. When the target test pressure is reached, the speed of the piston becomes zero. At this time, the output pressure of the booster pump is the target pressure and the components stop working. When the pressure of the high-pressure circuit drops due to temperature reduction and other reasons, the GLBP will automatically start to supplement the leakage pressure to keep the pressure in the circuit constant.

The GLBP is a reciprocating liquid booster device, whose booster element is mainly composed of two pistons, as shown in Fig. 5 (Wu et al., 2017; Li et al., 2018; Zhou et al., 2020). Air is used to drive the larger area of the piston for movement, and the smaller area of the piston is used to compress high-pressure water. According to the difference in the working pressure of the piston end face, the booster pump is divided into low-pressure driving components and high-pressure working components. The former include a pilot valve, a throttle valve and a reversing valve, while the latter encompass elements such as an inlet check valve and an outlet check valve. These components work together to convert air pressure to hydraulic pressure. The GLBP uses compressed air and water as the working medium, and the gas-liquid booster principle is pressurized by the piston area ratio of the cylinder and the hydraulic cylinder. Using the principle of pressure transfer and conversion, the device converts the energy exerted by low-pressure driving gas on a large-area piston into high-pressure clean water energy output on a small-area piston.

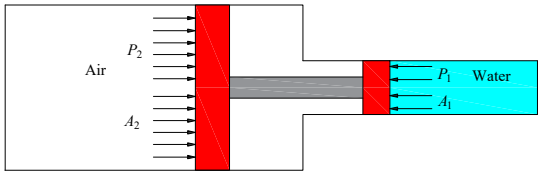

Fig. 5. Schematic diagram of gas-liquid pressurization.

On the basis of the force balance principle, the force balance equation is obtained:

$$P_1A_1 = P_2A_2 \tag{1}$$

where P_1 denotes the pressure of water on the high-pressure piston, MPa; P_2 denotes the pressure of air, MPa; A_1 denotes the pressure area of the high-pressure piston, mm^2; A_2 denotes the compression area of the low pressure piston, mm^2. The boost ratio is the area ratio of the two pistons:

$$I = \frac{P_1}{P_2} = \frac{A_2}{A_1} \tag{2}$$

where I represents the boost ratio.

According to the maximum pressure supply capacity of the test platform, which is 220 MPa, the driving pressure of the air can be selected as 0.85 MPa, so the pressurization ratio is about 258.8:1 according to Eq. (2). Relevant studies have pointed out that, in order to obtain the highest work efficiency, the maximum pressure supply capacity of the GLBP needs to be about 2/3 of the design pressure, so the design pressure is 330 MPa. The design boost ratio of the GLBP can be obtained from Eq. (3) as 388.2:1 and further rounded up to 400:1. The pressurization ratio can be altered by changing the ratio of the compression area A_1 and A_2. Therefore, the inner diameter of the hydraulic cylinder is selected as 8 mm, and the inner diameter of the gas cylinder is calculated as 160 mm.

$$\frac{I_D}{I} = \frac{3}{2} \tag{3}$$

where I_D represents the design boost ratio.

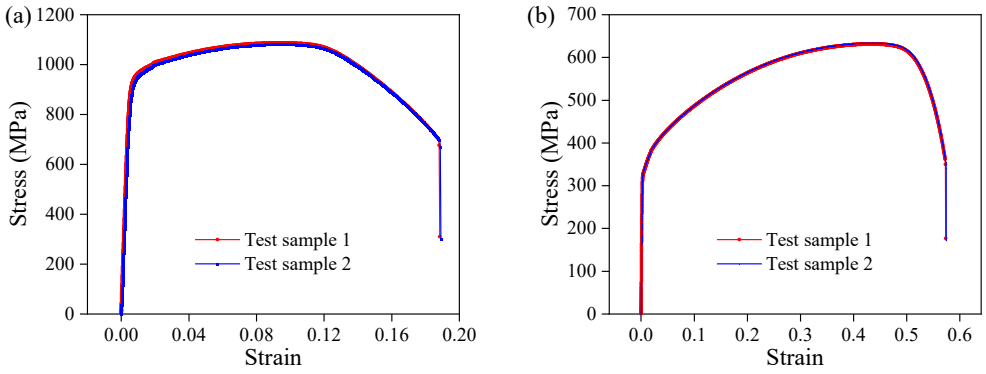

Fig. 6. Mechanical properties of the stainless steel material (a) 0Cr17Ni4Cu4Nb and (b) SUS304.

The main manufacturing material of the GLBP was 0Cr17Ni4Cu4Nb, whose yield strength is 925 MPa and tensile strength is 1,080 MPa, as shown in Fig. 6(a). The inner diameter of the high-pressure pipeline is 3 mm, and SUS304 stainless steel was used as the manufacturing material. The yield strength of the material is 330 MPa and the tensile strength is 633 MPa, as shown in Fig. 6(b).

The Faupel formula was used to calculate the wall thickness of the GLBP and high-pressure pipeline (Ding, 2014):

$$p_b = (2 - \frac{R_{p0.2}}{R_m}) \frac{2}{\sqrt{3}} R_{p0.2} \ln K \tag{4}$$

where p_b denotes the blasting pressure, MPa; $R_{p0.2}$ denotes the yield strength of the material, MPa; R_m denotes the tensile strength of the material, MPa; K denotes the ratio of outside diameter to inside diameter.

After taking a certain safety factor of the burst pressure, it can be used as the design pressure:

$$P(D) = \phi \frac{p_b}{n_b} \tag{5}$$

where $P(D)$ denotes the design pressure, MPa, and the maximum working pressure can be increased by 0.08 times to be used as the design pressure; ϕ denotes the decrease factor in the strength of the material at the design temperature, which is 1 because the pump does not operate at high temperature; n_b denotes the blasting safety factor, which is calculated according to the tensile test data as 3.

The expression for the logarithm of the diameter ratio is:

$$\ln K = \ln \frac{R_i + \delta}{R_i} \tag{6}$$

where R_i represents the inner diameter, mm; δ is the wall thickness, mm.

Accordingly, the calculation expression of wall thickness is further derived as:

$$\delta = \frac{D_i}{2} \left[\exp \left(\frac{\sqrt{3} n_b P(D)}{2\phi R_{p0.2} \left(2 - \frac{R_{p0.2}}{R_m}\right)} \right) - 1 \right] \tag{7}$$

where D_i denotes the inner diameter, mm.

Therefore, according to Eq. (7), the wall thickness of the high-pressure part of the pump can be calculated as 3.96 mm and the outer diameter as 17.92 mm, which is rounded up to 18 mm. The wall thickness of the high-pressure pipeline is 3.81 mm and the outer diameter is 10.62 mm, which is rounded up to 11 mm.

3.2 Heating and insulation module

The heating and insulation module consists of two parts: the temperature-controlled cabin and the EIHS, which work in unison to achieve the efficient application and maintenance of the set temperature. To realize the rapid rise of the temperature of the clean water inside the coring tool and avoid the water gasification caused by excessive temperature, the EIHS is used to circulate the high-temperature medium water. When the coring tool is evenly filled with high-temperature water, the temperature-controlled cabinet is used to further increase the temperature to the target value. Finally, the heating efficiency of the EIHS is improved to make the high-pressure water pumped by the GLBP reach the target test temperature required by the coring tool, and the temperature-controlled cabinet is further used to maintain the test temperature.

3.2.1 Temperature-controlled cabinet

The main body of the temperature-controlled cabinet is made of stainless steel, and its components are shown in Fig. 7. The coring tool is a cylinder with a maximum length of 4,900 mm and a maximum diameter of 280 mm. Considering the installation of the operating space, a rectangular experimental space with a length of 5,000 mm, a width of 350 mm and a height of 300 mm is set up inside the temperature-controlled cabinet for the installation of the fidelity coring tool. Furthermore, the application and maintenance of the required test temperature and pressure are completed in the testing space. A number of load-bearing beams are installed at the bottom of the experimental space, with a load-bearing capacity of more than 300 kg to meet the load-bearing requirements of the test of fidelity coring tools. At the same time, protective devices are installed in the experimental space to prevent contamination of the laboratory due to leaks. The upper cover of the space is composed of five cover plates, which reduce the weight of the cover plate and facilitate its opening for installation and disassembly of the coring tool. The sealing elements are used between each cover plate and the cabinet. The outer layer of the space is covered with thermal insulation material, which is ultrafine glass thermal insulation foam with a thickness of 50 mm. A high-pressure water inlet and a high-

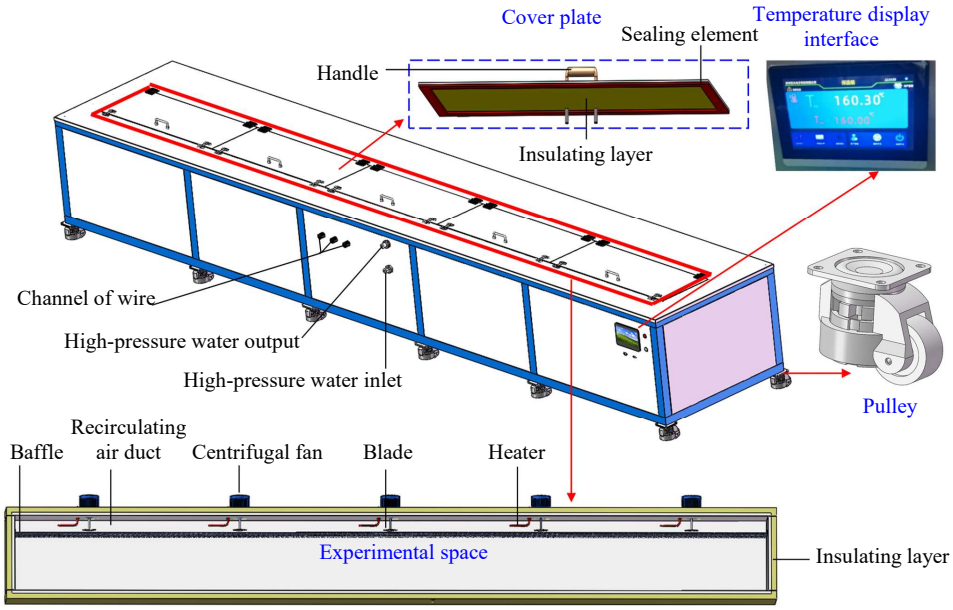

Fig. 7. Overall structure of the temperature-controlled cabinet.

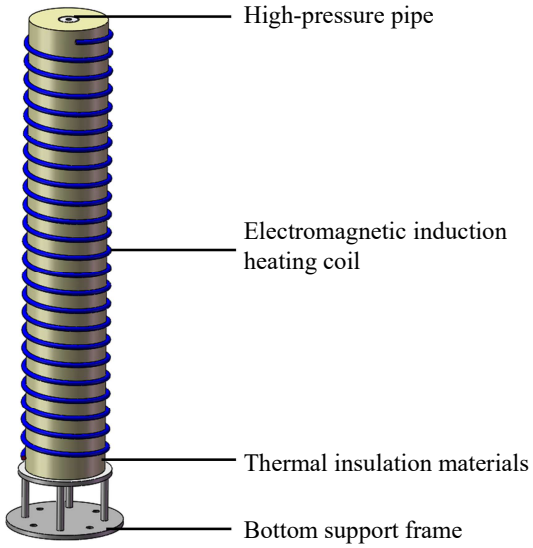

Fig. 8. Main components of the electromagnetic induction heating system.

pressure water outlet are fitted on the side wall of the cabinet, and three outlets are provided for the outgoing of the lead wires of the temperature sensor and pressure sensor. The outlets are covered with thermal insulation cotton. Pulleys are installed at the bottom of the temperature-controlled cabinet to facilitate the movement and maintenance of the cabinet.

The heating system of the temperature-controlled cabinet is installed on its back side and is composed of a recirculating air duct, five centrifugal fans and five heaters. The recirculating air duct is located between the baffle and the insulating layer in which the heater and the blade are distributed. The heater is heated at high speed by U-type nickel-chromium alloy electric heating wire, which is controlled by contactless constant period pulse width adjustable solid state relay. When the centrifugal fan is opened to make the wind blade rotate at high speed, the air in the studio is sucked into the air duct from the bottom, so that the air and the heat generated by the heater are fully mixed in the air duct and the heated gas is evenly blown out from the top of the studio. The heat in the air is exchanged with the test objects in the studio, and the exchanged air is sucked into the air duct for mixing and repeated circulation. Thus, the target temperature requirements can be achieved while ensuring that the test chamber has high temperature uniformity.

3.2.2 Electromagnetic induction heating system

The EIHS with a maximum heating power of 20 kW is installed on the high-pressure pipe near the temperature-controlled cabinet to quickly heat the clean water passing through the pipe. During the heating process, the temperature is controlled by adjusting the current, and the water temperature at the outlet is detected in real time to control the heating power. The EIHS mainly consists of heating coil, thermal insulation materials, bottom support frame, and high pressure pipe, as shown in Fig. 8. The high-pressure pipe is covered with thermal insulation materials, and the heating coil is wound around the outer side of the thermal insulation materials. The working principle of the EIHS is shown in Fig. 9. Cold water enters the EIHS from the left end of the pipe for heating, and the water heated to the target temperature is discharged from the right end of the pipe.

The working principle of the EIHS is as follows (Fu et al., 2012; Wang and Yan, 2024): The energy conversion of electromagnetic induction heating is a process in which magnetism is generated from electricity, then electricity is generated from magnetism, and then internal energy is generated in the conductor. When a changing AC current is passed through the wire, a changing electromagnetic field can be generated around the conductor coil, which can further induce the surrounding metal conductor and induce a current in the

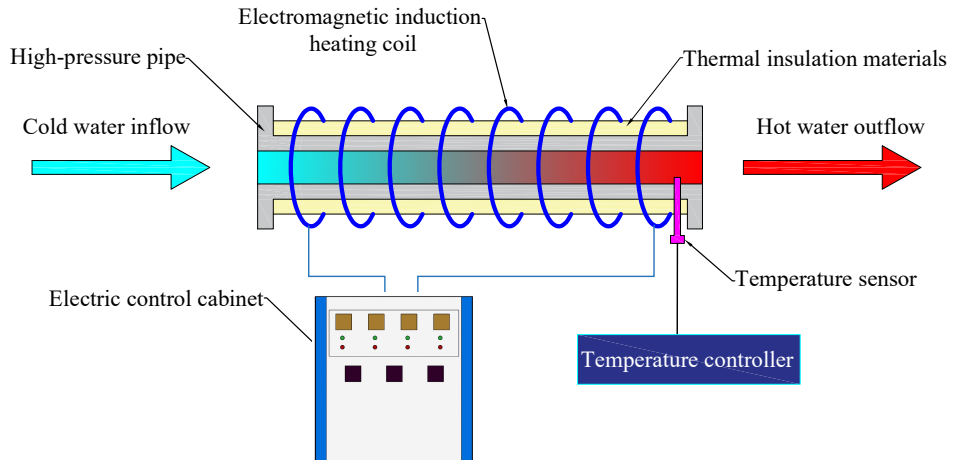

Fig. 9. Working principle of the electromagnetic induction heating system.

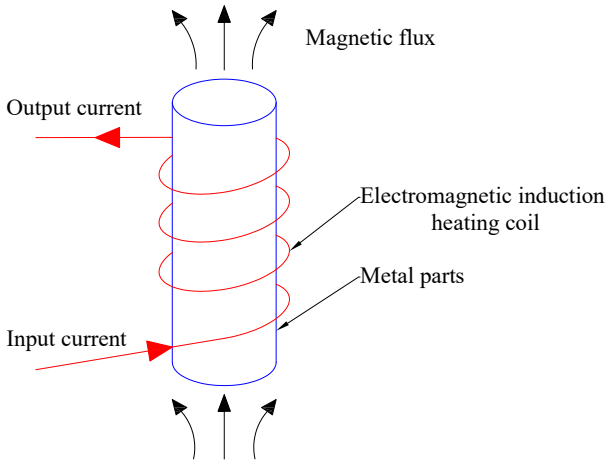

Fig. 10. The electromagnetic induction heating model.

conductor, also called eddy current. When the induced current flows in the conductor, the thermal effect of the conductor turns the electrical energy into internal energy, thus heating the conductor. The electromagnetic induction heating model is shown in Fig. 10.

The equation for calculating the induced electromotive force is as follows:

$$e = -\frac{\mathrm{d}\psi}{\mathrm{d}t} \tag{8}$$

where e denotes the induced electromotive force, V; ψ denotes the effective magnetic flux, Wb; t denotes time, s. Since the direction of the induced electromotive force is opposite to the direction of the magnetic flux change, a negative sign is added to the front of the expression.

It is assumed that the variation in the magnetic flux is a sinusoidal curve:

$$\psi = \psi_M \sin \omega t \tag{9}$$

where ω represents the angular frequency used to control the sinusoidal period, rad/s, $\omega = 2\pi f$, f denotes the frequency, Hz; ψ_M denotes the maximum magnetic flux, Wb.

From Eq. (8) and Eq. (9), it can be concluded that:

$$e = -2\pi f \psi_M \cos \omega t \tag{10}$$

It is further concluded that:

$$E = \frac{2\pi f \psi_M}{\sqrt{2}} \approx 4.443 f \psi_M \tag{11}$$

where E represents the effective value of the induced electromotive force, V.

It can be concluded from Eq. (11) that when the maximum value of magnetic flux is larger and the alternating frequency is higher, the corresponding induced electromotive force is larger.

When there is an induced electromotive force on the conductor, due to the conductivity of the conductor itself, the electrons in the conductor will move in a directional manner under the action of the induced electromotive force, and the current will be generated in the opposite direction of electron movement (Lucia et al., 2014; Broatch et al., 2017; Haldar and Lagoudas, 2018; Liu et al., 2018). Eddy current is a circle of closed loop current on the conductor. Because the metal conductor has resistance characteristics, it will consume electrical energy and convert the internal energy of the conductor, thus completing the electromagnetic heating process. The heat generated by electromagnetic induction is called Joule heat, which can be calculated as follows:

$$Q = Y^2 R t \tag{12}$$

where Q denotes the joule heat generated, J; Y denotes the current, A; R denotes the resistance of the conductor, Ω.

The power required for water heating from room temperature (calculated at 25 °C) to 160°C can be calculated according to Eq. (13). When the maximum flow rate of water is 3 L/min, the maximum power calculated is 28.35 W, so the maximum power of the EIHS is 28.35 W to meet the requirements of the equipment:

$$Q_w = C_w m(t_2 - t_1) \tag{13}$$

where Q_w denotes the heating power, W; C_w denotes the specific heat capacity of water, J/(kg·°C), calculated as 4,200

Fig. 11. Control panel of the measurement and control module. 1-Test status display area; 2-Data display area; 3-Test process control area; 4-Functional control area; 5-Status monitoring area.

J/(kg·°C); m denotes the mass of water flowing through the pipe in unit time, kg/s, $m = q \times \rho_w$, q is the flow rate of water, m^3/s, and the maximum value is 5×10^{-5} m^3/s; ρ_w denotes the density of water, which changes with the change of pressure and temperature, kg/m^3, and 1 kg/m^3 can meet the requirements in calculation; t_1 denotes the initial temperature value, which is 25 °C; t_2 denotes the target temperature, which is 160 °C.

3.3 Measurement and control module

The main functions of the measurement and control module include the data acquisition and automatic control of temperature and pressure. The control panel of the module is divided into five parts, which are test status display area, data display area, the test process control area, functional control area, and status monitoring area, as shown in Fig. 11. The test status display area is mainly used to display the on-off status of each valve in the whole platform in real time, and observe whether the function of each module is normal. The data display is mainly used to show the temperature and pressure values inside the coring tool, the water temperature at the outlet of the EIHS, the working temperature of the temperature-controlled cabinet, the start time of the experiment, and the total time used. At the same time, the change curve of temperature and pressure can also be drawn on the display. The time period on the curve can be selected by operating the mouse, and the curve can be amplified to observe the fluctuation of temperature and pressure in this time period. The test process control area is mainly used to control the temperature and pressure of the experiment, and the target value of the required temperature and pressure can be set in stages. The functional control area is mainly composed of various operation buttons of the system, including those for experiment information, save, open, system parameters, pressure relief start, close valve, clear alarm, and stop. The status monitoring area is mainly used for monitoring various states of the system, such as communication, emergency stop, start and stop, fault, and overpressure.

The measurement and control module uses sensors to collect and record the temperature and pressure data of each key part during the test process in real time and realizes the control of the test temperature and pressure according to the collected data. The layout scheme of the temperature and pressure sensors inside the coring tool is shown in Fig. 12. The pressure sensor is mounted on the transition of the fidelity coring tool and measures the pressure inside it. To ensure the uniformity of temperature inside the coring tool, three temperature sensors are uniformly arranged along the axis of the tool to directly measure its internal temperature, and the average value is used. Two temperature sensors are arranged on the temperature-controlled cabinet and the EIHS, respectively.

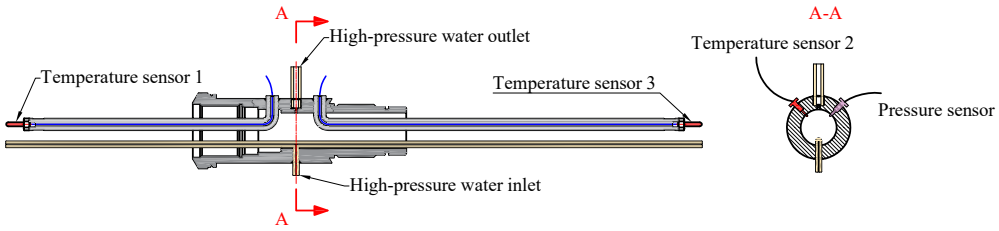

Fig. 12. Sensor layout of the fidelity coring tool.

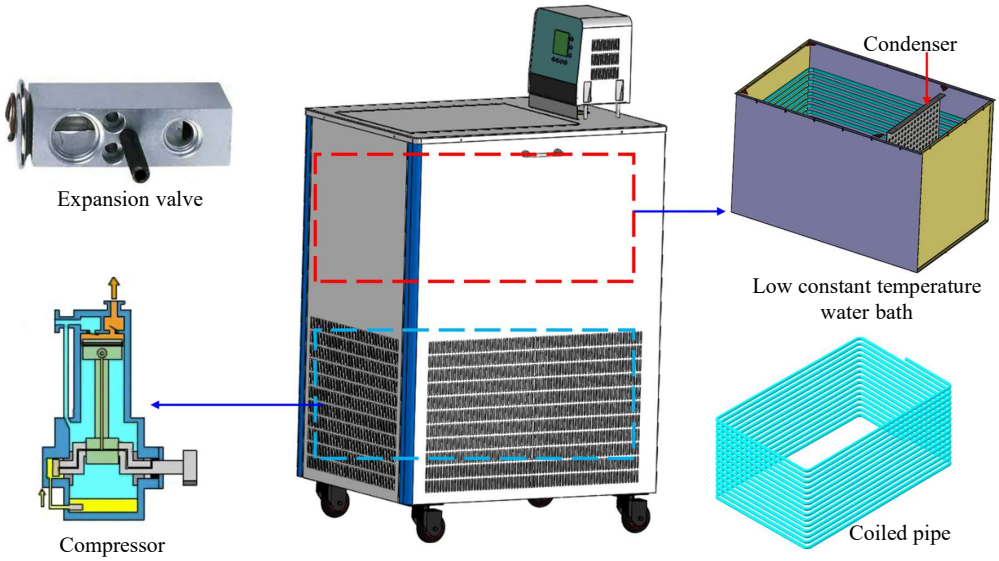

Fig. 13. Structure of the temperature-pressure unloading module.

3.4 Temperature and pressure unloading module

When the pressure of the system is released under high temperature and pressure, the overflow medium is high-temperature water, which will produce high-temperature water vapor and may cause accidents if it is not cooled down. The necessary cooling is achieved by the temperature-pressure unloading module before entering the tank. The temperature-pressure unloading module mainly consists of a low constant temperature water bath, a coiled pipe, a condenser, a compressor, and an expansion valve, as shown in Fig. 13. The low-temperature constant water tank is rectangular in shape. The cooling medium in the rectangular tank is ethylene glycol and the length of the cooling coil is 30 m. By adjusting the pressure inside the tank, the liquid glycol is evaporated into a gas to absorb heat, so that the water passing through the coil can be cooled. The glycol after gasification is compressed by the compressor, thus increasing its temperature. It further flows to the condenser to release heat and converts into a liquid, and finally returns to the tank after reducing the pressure through the expansion valve. The low-temperature and high-pressure water flows out from the outlet of the cooling coil, and the low-temperature and high-pressure water is discharged by the pressure reducing valve.

The cooling coil can increase the heat transfer area while reducing the space occupied by the equipment. According to the relevant theories of heat transfer, the heat transfer of the cooling coil can be calculated as follows:

$$Q' = kS\Delta t \tag{14}$$

where Q' denotes heat transfer, W; k denotes the total heat transfer coefficient, W/(m^2·°C); Δt denotes the logarithmic value of the average temperature difference of the cooling medium, °C; S denotes the heat transfer area, m^2.

According to the safe operating requirements of the equipment, the maximum flow rate of water is 3 L/min, the inlet temperature is 160 °C, and the outlet temperature is below 50 °C. Combined with Eq. (13), the minimum heat transfer rate is calculated as 23.1 W.

4. Experimental section

4.1 Experimental procedures

In order to ensure that the test platform can meet the testing requirements of fidelity coring tools, high-temperature and high-pressure tests were carried out on the test platform. First, the specimen installed in the experimental space of the temperature-controlled cabinet was a fidelity coring tool, with a total length of 3,160 mm, maximum outside diameter of 130 mm, and maximum inside diameter of 78 mm. Since the working pressure of the tool is 140 MPa and its working temperature is 150 °C, the performance test of the test platform under these conditions was carried out with this fidelity coring tool. Further, the specimen was replaced with high-pressure

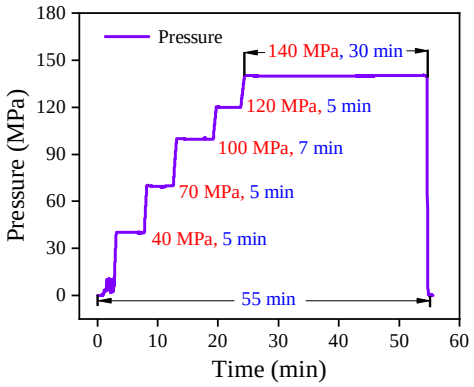

Fig. 14. Pressure-time curve with a maximum pressure of 140 MPa.

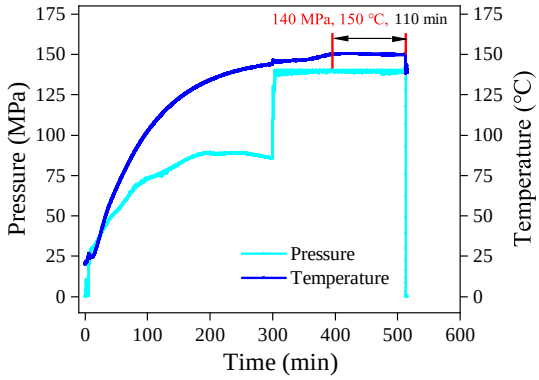

Fig. 15. Temperature-time and pressure-time curves at 140 MPa and 150 °C.

pipe to carry out a test under higher temperature and pressure, which verified the performance reliability of the test platform at 200 MPa and 160 °C, and the stability of the platform was further tested at the maximum pressure supply capacity of 220 MPa. The test process is shown below.

1) Complete the installation of specimens and all pipelines, and then leave the test site. Start the experiment and rely on the measurement and control module to start the GLBP. Pump the low-pressure circulating water. Meanwhile, the EIHS is controlled to make it start to work, and the circulating water is heated and further injected into the specimen to complete the discharge of air inside the specimen. Close the exhaust valve after the air has been discharged.
2) To improve heating efficiency, when the GLBP and the EIHS begin to operate, the temperature-controlled cabinet is started simultaneously to heat the air in the experimental space to the target test temperature. The hot air in the experimental space is continuously exchanged with the specimen until the temperature of the water inside the specimen reaches the target test temperature.
3) The heating power of the EIHS is further increased to raise the temperature of the water passing through it to the target test temperature. Start the GLBP again, pump the water flowing through the EIHS into the specimen, and raise the internal pressure of the specimen to the target pressure. Once the internal temperature and pressure of the specimen have stabilized at the target value, the heat preservation and pressure preservation experiment is carried out according to the test requirements.

4.2 Experiments based on a fidelity coring tool

4.2.1 High pressure test at 140 MPa

To ensure the safe operation of the entire test system, the high pressure experiment with a maximum pressure of 140 MPa was carried out in different pressure stages. The internal pressure curve of the coring tool versus time during the experiment is shown in Fig. 14. The pressure inside the coring tool was gradually increased to 140 MPa in five stages. During the first phase of increased pressure, the pressure was increased to 40 MPa, then it remained stable for 5 min. In the second pressure boost stage, the pressure was increased to 70 MPa. After 5 min of observation, the pressure remained stable. In the third pressure boost stage, the pressure was further increased to 100 MPa, and there was no change in pressure within 7 min. In the fourth pressure boost stage, the pressure was increased to 120 MPa, and there was no pressure drop or leakage after 5 min. Finally, the pressure was raised to the target pressure of 140 MPa. The Chinese standard GB150 points out that after reaching the target pressure during the pressure test, the pressure maintaining time should be no less than 30 min. The whole test system operated stably for 30 min under the maximum pressure of 140 MPa without any leakage of flow or pressure drop. That is, the pressure inside the coring tool remained stable throughout the experiment, and the test platform and fidelity coring tool showed good performance under a high pressure of 140 MPa.

4.2.2 Experiment at 140 MPa and 150 °C

On the basis of the high-pressure test results under 140 MPa, the experiment was further carried out under a pressure of 140 MPa and a temperature of 150 °C. The temperature and pressure curves of the water inside the fidelity coring tool during the experiment are shown in Fig. 15. After the internal pressure of the coring tool was increased from 0 to 30 MPa, the pressure increased with the temperature rising. At 300 min, the pressure inside the coring tool was raised to 140 MPa by the pump, and the system automatically maintained this pressure.

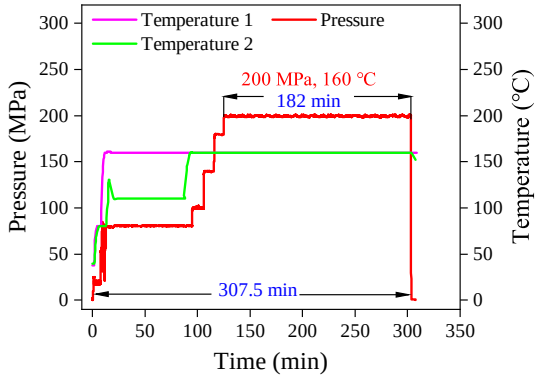

Fig. 16. Temperature-time and pressure-time curves at 200 MPa and 160 °C.

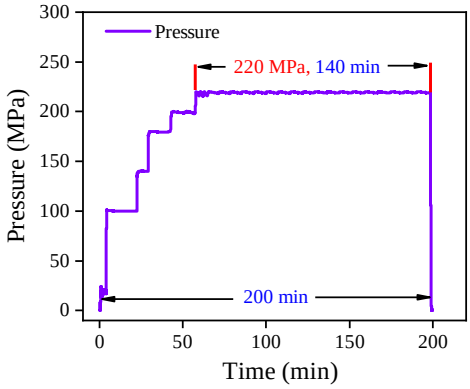

Fig. 17. Pressure-time curve at 220 MPa.

The water was further heated to the target temperature of 150 °C; thus, the target test temperature and pressure were applied. Finally, the internal pressure and temperature of the coring tool remained stable within 110 min, and the fluctuation was small. This indicates that the test platform and the fidelity coring tool had good performance at 140 MPa and 150 °C.

4.3 Maximum working performance test

To further test the ultimate working capacity of the test platform, experiments on the test platform under higher parameter values were carried out. First, a high-temperature and high-pressure experiment at 200 MPa and 160 °C was carried out. Then, to further verify the maximum pressure supply capacity of the test platform, a high pressure test with a maximum pressure of 220 MPa was carried out.

4.3.1 Performance test at 200 MPa and 160 °C

The test platform was subjected to an experiment lasting more than 3 h under the conditions of 200 MPa pressure and 160 °C temperature, and the test curve is shown in Fig. 16. Within a total of 83.7 min between 11.2 and 94.9 min, the temperature of each part of the test platform remained stable when the pressure was 80 MPa, the working temperature of the EIHS was 110 °C (Temperature 2), and the working temperature of the temperature-controlled cabinet was 160 °C (Temperature 1). The working temperature of the EIHS was further increased to 160 °C, and the pressure was increased from 80 to 200 MPa. Then, an experiment was conducted at 100 MPa and 160 °C for 11 min, at 140 MPa and 160 °C for 9.2 min, and at 180 MPa and 160 °C for 8.7 min. Finally, the pressure was increased to 200 MPa, and an experiment was carried out at 200 MPa and 160 °C for 182 min. There was no leakage or pressure drop during the test, that is, the temperature and pressure of the test platform remained stable, indicating good working performance. These experimental results confirm that the proposed platform can provide the test conditions of pressure of 200 MPa and temperature of 160 °C, which exceeds the test index of the fidelity coring tool.

4.3.2 Performance test at 220 MPa

The test platform was subjected to an experiment under a pressure of 220 MPa, during which the curve of pressure change over time was recorded, as shown in Fig. 17. Under the pressure condition of 220 MPa, no leakage was found after 140 min of pressure regulation test, which proves that the device has a pressure supply capacity of more than 200 MPa and can work under 220 MPa for an extended period, meeting the design requirements.

5. Conclusions

Taking the test requirements of deep *in-situ* fidelity coring tools as a basis, a high-pressure and high-temperature test platform was developed in this study, and its working performance was experimentally studied. The findings can be summarized as follows:

1) On the basis of the test requirements of fidelity coring tools, the overall structure scheme of the test platform was constructed, and the working principle of the test platform was introduced in detail.
2) The maximum working pressure of the pressurization module was determined as 220 MPa, which exceeds the working pressure index of the test platform. The temperature-controlled cabinet and the electromagnetic induction heating system works together in unison to realize the rapid application of the test temperature of 160 °C. The measurement and control module can automatically monitor and control the temperature and pressure during the test. After the experiment, the platform can automatically realize the safe unloading of temperature and pressure.
3) A fidelity coring tool was used to complete the test at a pressure of 140 MPa and a temperature of 150 °C inside the test platform. The temperature and pressure remained stable during the experiment. After experimental research for more than 182 min under a pressure of 200 MPa and a temperature of 160 °C, the platform exhibited good working performance. After a 140 min test under the maximum pressure of 220 MPa, there was no leakage or pressure drop.
4) The proposed test platform can provide an effective means of testing in the research of deep *in-situ* fidelity coring tools and can be further used to explore the bearing capacity and related mechanical properties of coring tools under high-temperature and high-pressure environments. This is of significant value for the safe mining of deep resources and the accurate evaluation of deep resource reserves.

Acknowledgements

This work was supported by the National Natural Science Foundation of China (Nos. 52225403, 52104096, 52304033), the Guangdong Provincial Key Laboratory of Deep Earth Sciences and Geothermal Energy Exploitation and Utilization (No. DESGEEU-2023-6), and the China Postdoctoral Science Foundation (No. 2023M742446).

Conflict of interest

The authors declare no competing interest.

References

Broatch, A., Olmeda, P., Garcia, A., et al. Impact of swirl on in-cylinder heat transfer in a light-duty diesel engine. Energy, 2017, 119: 1010-1023.

Ding, G. Design and research on simulation test shaft of high temperature and high pressure. Qingdao, China University of Petroleum (East China), 2014.

Dou, Y., Han, S., Zheng, J., et al. Development status of domestic high temperature and high pressure downhole tool testing equipment. Petrochemical Industry Application, 2022, 41(1): 1-6, 26. (in Chinese)

Du, J., Wei, L. Design of high-temperature and high-pressure environment simulation device. Advances in Intelligent Systems Research, 2015, 25: 62-67.

Fu, Y., Zhou, H., Wang, J., et al. Analysis of crack arrest by electromagnetic heating in metal with oblique-elliptical embedding crack. Key Engineering Materials, 2012, 525-526: 405-408.

Gao, M., Hao, H., Xue, S., et al. Discing behavior and mechanism of cores extracted from Songke-2 well at depths below 4,500 m. International Journal of Rock Mechanics and Mining Sciences, 2022, 149: 104976.

Gao, M., Xie, J., Gao, Y., et al. Mechanical behavior of coal under different mining rates: A case study from laboratory experiments to field testing. International Journal of Mining Science and Technology, 2021, 31(5): 825-841.

Guo, D., Li, J., Wang, D., et al. Structural improvement of differential motion assembly in in situ pressure-preserved coring system using CFD simulation. Applied Sciences-Basel, 2023, 13(7): 4108.

Haldar, K., Lagoudas, D. C. Dynamic magnetic shape memory alloys responses: Eddy current effect and joule heating. Journal of Magnetism and Magnetic Materials, 2018, 465(1): 278-289.

He, Z., Xie, H., Gao, M., et al. Research on properties of hollow glass microspheres/epoxy resin composites applied in deep rock *in-situ* temperature-preserved coring. Petroleum Science, 2022, 19(2): 720-730.

Hooker, P. R., Brigham, W. E. Temperature and heat transfer along buried liquids pipelines. Journal of Petroleum Technology, 1978, 30(5): 747-749.

Huang, W., Li, J., Liu, Z., et al. Study of a low-disturbance pressure-preserving corer and its coring performance in deep coal mining conditions. International Journal of Mining Science and Technology, 2023, 33(11): 1397-1410.

Kabir, C. S., Hasan, A. R., Jordan, D. L., et al. A wellbore/reservoir simulator for testing gas wells in high-temperature reservoirs. SPE Formation Evaluation, 1996, 11(02): 128-134.

Li, C., Luo, X., Zhang, L., et al. Numerical calculation and analysis of gas-liquid two-phase flow in a centrifugal multiphase pump for deep-sea mining. IOP Conference, 2018, 163: 012045.

Li, C., Xie, H., Gao, M., et al. Novel designs of pressure controllers to enhance the upper pressure limit for gas-hydrate-bearing sediment sampling. Energy, 2021, 227: 120405.

Liu, H., Ma, H., Zeng, L., et al. High temperature and high pressure downhole tool test system. China Petroleum Machinery, 2019, 47(12): 100-105. (in Chinese)

Liu, W., Feng, Y., Yang, T., et al. Analysis of the induction heating efficiency and thermal energy conversion ability under different electromagnetic stick structures in the RPECT. Applied Thermal Engineering, 2018, 145: 277-286.

Lucia, O., Maussion, P., Dede, E. J., et al. Induction heating technologyand its applications: Past developments, current technology, and future challenges. IEEE Transactions on Industrial Electronics, 2014, 61(5): 2509-2520.

Pang, D., Wang, Z., Pan, D., et al. Development of high temperature and high pressure downhole tool test device. Well Testing, 2017, 26(4): 45-48, 51, 77. (in Chinese)

Walker, M. Pushing the extended-reach envelope at sakhalin: An Operator experience drilling a record reach well. Paper SPE 151046 Presented at IADC/SPE Drilling Conference and Exhibition, California, 6-8 March, 2012.

Wang, B., Yan, M. Research on the heating effect evaluation of the electromagnetic induction heating system at low temperature based on the electrochemical-thermal coupling model. Journal of Energy Storage, 2024, 87: 111348.

Wu, T., Liu, J., Zhang, L., et al. Experimental study on multi-stage gas-liquid booster pump for working fluid pressurization. Applied Thermal Engineering, 2017, 126: 9-16.

Xie, H., Gao, M., Zhang, R., et al. Application prospects of deep *in-situ* condition-preserved coring and testing systems. Advances in Geo-Energy Research, 2024, 14(1): 12-24.

Xie, H., Liu, T., Gao, M., et al. Research on *in-situ* condition preserved coring and testing systems. Petroleum Science, 2021, 18(6): 1840-1859.

Wei, Z., He, Z., Yang, J. Analysis of core temperature variation and its influencing factors in deep rock *in-situ* temperature-preserved coring. Advances in Geo-Energy Research, 2024, 14(3): 215-223.

Yang, X., Xie, H., Chen, L., et al. Assembly process analysis and system design for deep *in-situ* fidelity corer. Advanced Engineering Informatics, 2024, 62: 102562.

Yu, B., He, Z., Yang, J., et al. Innovative Design of a Conductive Center Pole for an Active Thermal Insulation and Coring System in Deep Rock. Applied Science-Basel, 2023, 13(3): 1242.

Zhang, F. Development of drilling tool test system in Dagang oilfield. Oil Field Equipment, 2009, 38(1): 72-78. (in Chinese)

Zheng, J., Zong, Y., Qian, D., et al. Development of downhole environment simulation test equipment. Science Technology and Engineering, 2017, 17(8): 21-25. (in Chinese)

Zhou, L., Han, Y., Lv, W., et al. Numerical calculation of energy performance and transient characteristics of centrifugal pump under gas-liquid two-phase condition. Micromachines, 2020, 11(8): 728.